Letter

Diagnosing phase transitions through timescale entanglement

Stefan Rohshap,[1,*] Hirone Ishida,[2] Frederic Bippus,[1] Leonard M. Verhoff,[1] Anna Kauch,[1] Karsten Held,[1] Hiroshi Shinaoka,[2] and Markus Wallerberger[1]

[1]*Institute of Solid State Physics, TU Wien, 1040 Vienna, Austria*

[2]*Department of Physics, Saitama University, Saitama 338-8570, Japan*

(Received 17 July 2025; revised 2 October 2026; accepted 6 October 2026; published 17 November 2026)

Spatial entanglement of quantum states has become a central paradigm of many-body physics. Here, we unearth a fundamentally different form of entanglement, the entanglement between imaginary timescales. This timescale entanglement is accessible through quantics tensor train diagnostics (QTTD), where the bond dimension of an n-particle correlator encodes the coupling between temporal scales. Our central result is that timescale entanglement is generically enhanced in the vicinity of phase transitions and crossovers. At quantum critical points, it becomes scale invariant. We demonstrate timescale entanglement across a range of systems, including finite-size Hubbard rings, the transverse-field Ising model, the single-impurity Anderson model, and the Mott transition in the Hubbard model. Remarkably, the enhanced timescale entanglement is largely independent of the specific observable, establishing QTTD as a universal and unbiased diagnostic of criticality.

DOI: 10.1103/znzs-rccp

Introduction. Phase transitions are among the most intriguing phenomena in physics. Yet, their numerical treatment and detection can be challenging, especially when exotic phases emerge [1–3]. In extended many-body systems, the full wave function is usually not available, and using susceptibilities to diagnose transitions can be brittle, since we need to know *a priori* where to look, i.e., we must make sure to compute the response associated with the transition in question or at least one that is not insensitive to the transition. In general, we can expect some, but a much weaker, signal in the susceptibilities that are not the one associated with the symmetry breaking for a second-order phase transition. On the other hand, susceptibilities generally provide less clear precursors near first-order phase transitions.

Similarly, entanglement is one of the most enigmatic quantum phenomena. It is challenging to calculate in true many-electron systems where many electrons contribute and are entangled [4–10]. In (quasi-)one-dimensional spin systems, matrix product states (MPS) [11,12] have unlocked much of the theoretical and numerical analysis of entanglement [13,14] and its growth [15–17]. MPS add to the physical space an auxiliary, *latent* space, whose dimension ("bond dimension") indicates the strength of spatial entanglement [18,19].

Recently, it was shown that the machinery of MPS can be reused to compactify arbitrary functions in space and time [20–24]. Instead of a physical spin at some site, each tensor represents a different time/length scale of the function, so as we step along the train, we zoom in and out rather than move left or right. This ansatz was termed the quantics tensor train (QTT). It was instrumental in breaking computational barriers in modeling turbulence [25–29], plasmas [30], quantum chemistry [31], and—most relevant to this Letter—electronic correlation functions. In this latter case, some of us showed how to sample [32], store [33], and perform calculations [34] with electronic response functions which were previously inaccessible. QTTs by construction also feature a latent space and an associated bond dimension, which has hitherto been chiefly used as a measure of performance.

In this Letter, we reason by analogy with MPS, where the bond dimension gauges spatial entanglement: we propose the QTT bond dimension of electronic functions as a physical measure, namely, as the strength of time and length scale entanglement. For the example of the Hubbard dimer, we plot this over different timescales in Fig. 1(c).

Here, we observe that timescale entanglement is maximal at crossovers and phase transitions [red dots in Fig. 1(b)]. These maxima can appear in both single- and two-particle propagators [Fig. 1(b)], without the need to identify the specific susceptibility associated with the transition. We call this program of detecting phase transitions *quantics tensor train diagnostics* (QTTD). Additional results and details supporting the conclusions reached for all models discussed are provided in the Supplemental Material (SM) [35].

Quantics tensor trains. In QTTs [20,33] each variable is represented through a set of binary numbers or "quantics" corresponding to different length or timescales. The resulting tensor is then factorized into a tensor train (TT) at each scale. For illustration, consider a function $f(\tau)$ of a discretized variable τ, with $\tau \in \{0, \ldots, M-1\}$ on $M = 2^R$ grid points. In quantics, τ is expressed in binary representation $\tau = (\sigma_1 \sigma_2 \ldots \sigma_R)_2 = \sum_{\ell=1}^{R} 2^{R-\ell} \sigma_\ell$, with $\sigma_\ell \in \{0, 1\}$ leading to $f(\tau)$ being seen as a $2 \times 2 \times \cdots \times 2$ (R times) tensor $F_{\sigma_1, \ldots, \sigma_R}$ instead. Now each tensor index σ_ℓ corresponds to an

*Contact author: stefan.rohshap@tuwien.ac.at

Published by the American Physical Society under the terms of the Creative Commons Attribution 4.0 International license. Further distribution of this work must maintain attribution to the author(s) and the published article's title, journal citation, and DOI.

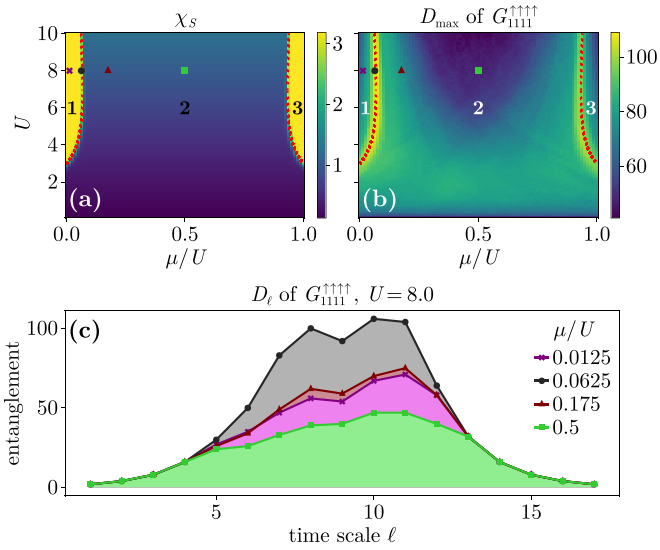


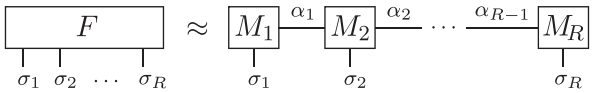
FIG. 1. Entanglement of exponentially different imaginary timescales for the Hubbard dimer at $T = 0.02$: (a) Local spin susceptibility χ_s indicating different ground states filled with one, two, and three electrons; (b) QTT maximum bond dimension $D_{\max} := \max_\ell D_\ell$ of the imaginary-time four-point Green's function $G^{\uparrow\uparrow\uparrow\uparrow}_{1111}$ as a function of interaction strength U and chemical potential μ/U, where red-dashed lines mark crossings of the ground state; and (c) QTT bond dimension D_ℓ between timescale $2^{-\ell}$ and $2^{-\ell-1}$ for different values of μ/U at $U = 8$, marked by the same symbol and color in (a) and (b).

exponentially distinct length or timescale of the system. The first bit σ_1 represents the coarsest scale that divides the system into halves, while the last bit σ_R reflects the finest scale.

Factorization of this tensor into a (truncated) TT or matrix product state (MPS) of the form

$$F_{\sigma_1\ldots\sigma_R} \approx \tilde{F}_{\sigma_1\ldots\sigma_R} = \sum_{\alpha_1=1}^{D_1} \cdots \sum_{\alpha_{R-1}=1}^{D_{R-1}} [M_1]^{\sigma_1}_{1\alpha_1} [M_2]^{\sigma_2}_{\alpha_1\alpha_2} \cdots [M_R]^{\sigma_R}_{\alpha_{R-1}1} \tag{1}$$

can be achieved with singular value decomposition (SVD) [33,36] or using tensor cross interpolation (TCI) [32,37–39]. In Eq. (1), each M_ℓ is a $D_{\ell-1} \times 2 \times D_\ell$ tensor with "physical" binary index σ_ℓ and virtual indices ("bonds") $\alpha_{\ell-1}, \alpha_\ell$, which are summed over. Equation (1) translates to



(2)

in tensor network form [12]. We define the (maximum) bond dimension of the QTT as $D_{\max} = \max_\ell(D_\ell)$. Generally, bond dimensions D_ℓ characterize the flow of information between different timescales (as well as length scales) and, thus, the amount of "length or timescale entanglement" in the system up to some precision ϵ [40]. In the case of SVD, usually the squared Frobenius norm $\epsilon = ||F - \tilde{F}||^2_{\mathrm{F}}/||F||^2_{\mathrm{F}}$ is taken as a measure of the error of the approximation in Eq. (1). Many problems in many-body physics have been shown to use quantities that are strongly compressible into QTTs with small bond dimension [32–34,40–49] or name the application of QTTs to overcome bottlenecks in the future [50,51].

Quantics tensor train diagnostics. Let us start from a general imaginary-time two-point correlator $G_{AB}(\tau) = -\langle \hat{\mathcal{T}} \hat{A}(\tau) \hat{B} \rangle$ with fermionic operators $\hat{A}, \hat{B}$ and the time-ordering operator $\hat{\mathcal{T}}$. For a finite or gapped system, $G_{AB}(\tau)$ can be expressed in its Lehmann representation,

$$G_{AB}(\tau) = -\frac{1}{Z} \sum_n e^{-\beta\epsilon_n} \sum_m e^{-\tau(\epsilon_m - \epsilon_n)} \langle n|\hat{A}|m\rangle \langle m|\hat{B}|n\rangle, \tag{3}$$

where $1/\beta$ is temperature, $\tau \in [0, \beta)$ is imaginary time, Z is the partition function, $\hat{H}$ is the Hamiltonian including the chemical potential, and $\hat{H}|n\rangle = \epsilon_n|n\rangle$ defines its eigenenergies and eigenstates. Clearly, $G_{AB}(\tau)$ is the sum of exponentials. An exponential has a QTT representation of bond dimension one, since it is a product of exponentials of the binary variables σ_ℓ at each scale: $e^{\tau\epsilon} = \prod_{\ell=1}^{R} e^{\epsilon\beta 2^{-\ell}\sigma_\ell}$. The bond dimension of the exact QTT representation of G_{AB} is thus bound by the number of nonzero elements in the sum. Let us now consider the case of temperature approaching zero ($\beta \to \infty$), then

$$G_{AB}(\tau) = -\frac{1}{N} \sum_{i=1}^{N} \sum_m (e^{-\tau\epsilon_m} \langle \mathrm{GS}_i|\hat{A}|m\rangle \langle m|\hat{B}|\mathrm{GS}_i\rangle + e^{-(\beta-\tau)\epsilon_m} \langle m|\hat{A}|\mathrm{GS}_i\rangle \langle \mathrm{GS}_i|\hat{B}|m\rangle), \tag{4}$$

where $|\mathrm{GS}_i\rangle$ denotes the ith ground state and N is the number of ground states (states with the lowest energy). We set $\epsilon_{\mathrm{GS}} = 0$, and the first (second) term contributes predominately for small (large) values of τ.

For a single nondegenerate ground state, the bond dimension of the exact QTT representation is bounded by the number of nonzero terms in the sum, maximally by $M - 1$ for M eigenstates m. Next, consider a ground-state crossing of the two lowest states $|\mathrm{GS}_1\rangle$ and $|\mathrm{GS}_2\rangle$ ($N = 2$). Then, the bond dimension of the exact QTT is at most $2M - 2$ since twice as many exponentials can contribute. In practice, it may be lower as fewer states $|m\rangle$ will give nonzero matrix elements. Still, at the ground-state crossing the sum consists of the exponentials and matrix elements associated with $|\mathrm{GS}_1\rangle$ and $|\mathrm{GS}_2\rangle$ leading to larger bond dimensions of $G_{AB}(\tau)$ than before or after the crossing, as long as $\hat{A}$ and $\hat{B}$ are not completely orthogonal to the response of the system. Therefore, at zero temperature, a ground-state crossing in finite systems can be determined by monitoring the bond dimension of the QTT representation. We call this approach quantics tensor train diagnostics, where the diagnostics power of the approach is further examined in Sec. I of the SM [35].

Consider finite but low temperatures. Then, also excited states $|n\rangle$ contribute to $G_{AB}(\tau)$, suppressed by $e^{-\beta\epsilon_n}$. Most of these contributions will be truncated if they are below a certain specified cutoff in the QTT construction of the two-point correlator. Hence, we will still see a peak of $D_{\max}$ in the vicinity of the corresponding crossing (at $T = 0$) that will be smeared out with increasing temperature.

We can summarize the QTTD procedure in the following way. (1) Calculate an available correlator of the system. (2) Vary the QTT cutoffs and analyze the bond-dimension profile to find stable features corresponding to possible phase

transitions or crossovers. (3) Iterate this procedure for different available correlators to verify the obtained maxima as universal features corresponding to the system-inherent rise in timescale entanglement associated with a phase transition or crossover.

In the following, we use the notion of imaginary time and Matsubara frequency scale entanglement interchangeably, as both representations are related by a Fourier transform and encode the same underlying multiscale structure of the correlation functions. Before investigating genuine phase transitions in extended systems, let us first verify the validity of this derivation in simple finite systems.

Hubbard model. We start by introducing the Hubbard model on N sites:

$$\hat{H} = -\sum_{\sigma}\sum_{i,j=1}^{N} t_{i-j}\hat{c}^{\dagger}_{i,\sigma}\hat{c}_{j,\sigma} + \sum_{i=1}^{N}(U\hat{n}_{i,\uparrow}\hat{n}_{i,\downarrow} - \mu(\hat{n}_{i,\uparrow}+\hat{n}_{i,\downarrow})), \tag{5}$$

where $t_{\pm 1} \equiv t$ and $t_{\pm 2} \equiv t'$ are the nearest and next-nearest hopping amplitude, respectively; all other hopping amplitudes are set to zero; the local on-site Coulomb interaction is U; the chemical potential is μ; and the number operators $\hat{n}_{i,\sigma} = \hat{c}^{\dagger}_{i,\sigma}\hat{c}_{i,\sigma}$ are defined via the fermionic annihilation (creation) operators $\hat{c}^{(\dagger)}_{i,\sigma}$ with $\sigma = \uparrow, \downarrow$ and site index i. We use $t \equiv k_B \equiv 1$ to set energy and temperature units.

Hubbard dimer. For the Hubbard dimer [1D, $N = 2, t' = 0$ in Eq. (5)], all 16 eigenstates can be analytically calculated [52], providing a first good test case for QTTD. Figure 1(b) shows $D_{\max}$ of the local two-particle Green's function $G^{\uparrow\uparrow\uparrow\uparrow}_{1111}(\tau_1,\tau_2,\tau_3) = -\langle \mathcal{T}\hat{c}_{1,\uparrow}(\tau_1)\hat{c}^{\dagger}_{1,\uparrow}(\tau_2)\hat{c}_{1,\uparrow}(\tau_3)\hat{c}^{\dagger}_{1,\uparrow}\rangle$ with $\epsilon = 10^{-14}$ at $\beta = 50$ and $R = 6$. As expected, a sharp peak in $D_{\max}$ can be seen in the vicinity of the ground-state crossing, indicated by dashed lines. Here, the singlet ground state crosses with a doublet that has one (three) electrons at small (large) values of μ/U. In Fig. 1(a), the value of the spin susceptibility χ_S (definition in Sec. II of the SM [35]) is shown, clearly distinguishing the two "phases." Figure 1(c) plots the bond dimension as timescale entanglement measure over the imaginary timescale. Additionally, we extend the analysis to four-site Hubbard rings with and without next-nearest-neighbor hoppings [53] in the SM [35]. Besides varying QTT cutoffs to identify ground-state crossings and thermal crossovers, various entanglement measures [9,54–76] are analyzed in the SM [35].

Quantum criticality in transverse-field Ising model. At a quantum phase transition (QPT), the system becomes scale invariant in both spatial and imaginary-time directions. In the absence of a characteristic scale, fluctuations span all temporal scales, resulting in comparable contributions from coarse and fine scales to the system's response. In the following, we investigate how this emergent scale invariance manifests itself in the structure of timescale entanglement in the vicinity of the QPT of the one-dimensional transverse-field Ising model (TFIM), described by $\hat{H} = -\sum_{i=1}^{L}(J\hat{\sigma}^x_i\hat{\sigma}^x_{i+1} + h\hat{\sigma}^z_i)$ with the spin operators $\hat{\sigma}^{\alpha}_i$, nearest-neighbor spin coupling J, and a transverse field h. At zero temperature, the model exhibits a continuous quantum phase transition between ferromagnetic and paramagnetic phases at $J = h$, where the system becomes

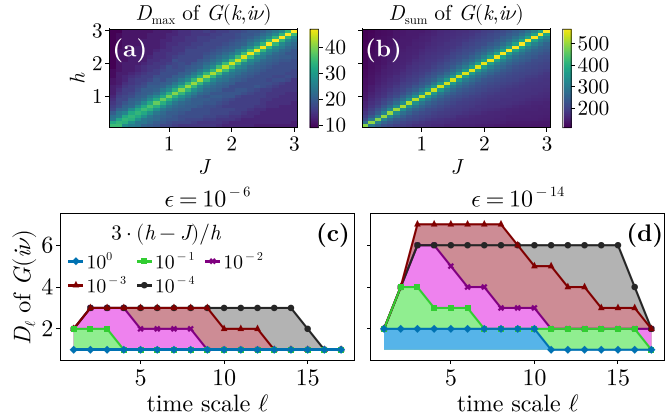


FIG. 2. $D_{\max}$ (a) and D_{sum} (b) of $G(k, i\nu)$ of the TFIM for $R = 12$, $\epsilon = 10^{-14}$ at $\beta = 10^4$. (c), (d) Bond-dimension profile D_ℓ of local Green's function $G(i\nu)$ at $\beta = 10^7$ near criticality ($h = 3$). Criticality and scale invariance lead to uniform entanglement across logarithmic timescales independent of ϵ.

scale invariant in both spatial and imaginary-time directions. Exploiting the exact analytical solution for the normal Green's function $G(k, i\nu)$ (see Sec. VIII of the SM [35] or Ref. [77]), we perform a QTT compression at very low temperature ($\beta = 10^4$). As shown in Figs. 2(a) and 2(b), both the maximum bond dimension $D_{\max}$ and, more prominently, the sum of bond dimensions, $D_{\text{sum}} := \sum_\ell D_\ell$, which quantifies the total coupling between scales, exhibit clear peaks at the critical point $J = h$. This reflects the increasing complexity of the correlation structure as the system approaches criticality, where contributions from all scales become relevant. A physically interesting signature of criticality emerges in the bond-dimension profile of the local Green's function $G(i\nu)$ at ultralow temperatures ($\beta = 10^7$) very close to the QPT. As shown in Figs. 2(c) and 2(d), the bond dimensions become nearly independent of the timescale ℓ, indicating that all imaginary timescales contribute equally when approaching criticality. This flattening of the bond-dimension profile constitutes a direct numerical manifestation of scale invariance: the absence of a characteristic temporal scale at the QPT is encoded as a uniform distribution of entanglement across logarithmic timescales. Notably, this behavior is robust with respect to the QTT compression threshold ϵ, affecting only the overall magnitude of the bond dimensions but not their scale-independent structure. These findings are closely connected to earlier results for critical quantum systems, where entanglement grows logarithmically with system size, reflecting an organization of correlations across length scales that is naturally captured by the multiscale entanglement renormalization ansatz (MERA) [78–86]. In this context, our results suggest an analogous multiscale organization in imaginary time, directly revealed through QTT bond dimensions.

Mott transition. Next, we investigate whether timescale entanglement, as captured by QTT decompositions, can diagnose phase transitions in realistic many-body calculations. To this end, we analyze the first-order Mott metal-to-insulator transition present in the dynamical mean-field theory (DMFT) [87–90] solution of the Hubbard model on the Bethe lattice. Using data from Refs. [91,92], we construct the particle-hole

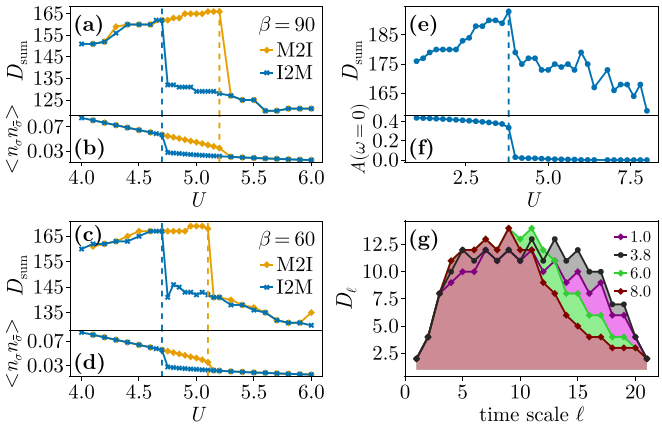


FIG. 3. Sum of QTT bond dimensions of $G(i\nu)G(i\nu + i\omega)$ obtained from DMFT solution for the Bethe lattice for $\beta = 90$ (a) and 60 (c) initialized in insulating (I2M) and metallic (M2I) states vs the double occupancy $\langle n_\sigma n_{\bar{\sigma}} \rangle$ (b) and (d) for various U in units of $t = 1$. (e) D_{sum} of same property for 3D $NdNiO_2$ at $\beta = 38\,\text{eV}^{-1}$ in comparison to analytically continued spectral weight $A(\omega)$ at $\omega = 0$ in (f). (g) Bond-dimension profile for various U, with spread of timescale entanglement to fine scales at crossover ($U = 3.8\,\text{eV}$). QTT parameters: $R = 11$, $\epsilon = 10^{-4}$.

bubble $G(i\nu)G(i\nu + i\omega)$ [93] and compress it into a QTT via SVD. Figures 3(a) and 3(c) show the resulting D_{sum} obtained from DMFT solutions initialized in the insulating (I2M) and metallic (M2I) states at $\beta = 90$ and 60, respectively, as a function of the interaction strength U. In both cases, pronounced peaks in D_{sum} appear at different values of U, coinciding with steep drops in the double occupancy [Figs. 3(b) and 3(d)] that mark the onset of the insulating regime. In contrast to a QPT, a finite-temperature first-order transition is characterized by the coexistence of distinct phases with finite correlation lengths and, hence, well-defined characteristic scales. No scale invariance emerges in this case. However, timescale entanglement is enhanced when approaching the phase transition, both from the metallic and insulating regimes. For a more concise picture, we refer the reader to Fig. 20 in the SM [35] showing an extended U-range.

We next extend the analysis to a realistic material computation. Figure 3(e) shows D_{sum} of the same bubble quantity computed for three-dimensional (3D) $NdNiO_2$ [94] within (single-orbital) DMFT calculation with density functional theory input [90,95–97] at $\beta = 38\,\text{eV}^{-1}$ and half-filling, as a function of U, alongside the analytically continued [98] spectral weight $A(\omega)$ at $\omega = 0$ in Fig. 3(f). In contrast to the Bethe lattice at lower T (with respect to bandwidth), no hysteresis is observed. Instead, D_{sum} exhibits a single pronounced peak that coincides with the suppression of $A(\omega = 0)$, signaling a crossover from metallic to insulating behavior. At this crossover ($U \approx 3.8$), the bond-dimension profile [Fig. 3(g)] reveals a more uniform distribution across scales, indicating enhanced entanglement between imaginary timescales [99]. We interpret this observation in the following way. In crossover regimes, no singular behavior or diverging correlation length is present. Instead, spectral weight and correlations are continuously redistributed across energy and timescales, leading to broader and less pronounced increases in entanglement of temporal scales. However, near underlying critical points this redistribution can involve a broad range of scales. Especially in the vicinity of a finite-temperature second-order phase transition, the emergence of scale invariance in the spatial degrees of freedom may induce broad multiscale structures in imaginary time, which are encoded in the corresponding correlation functions. As a result, temporal correlations become distributed across a wider range of scales, leading to a partial flattening of the bond-dimension profile reflecting the increase of entanglement between temporal scales. Therefore, QTTD suggests a route to probing how scale invariance is encoded in generic observables through enhanced coupling between imaginary timescales.

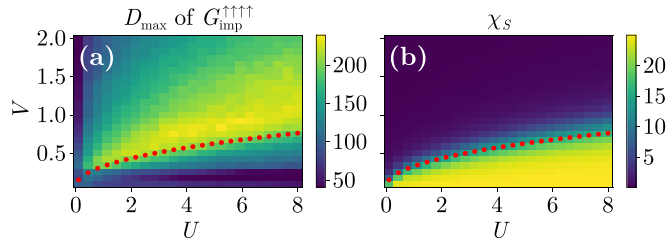


FIG. 4. (a) D_{max} of two-particle Green's function of SIAM ($\beta = 100$) in $U - V$ plane [red dots indicate $T_K(U, V) = 1/\beta$]. (b) Spin susceptibility χ_S indicating different regimes.

Single-impurity Anderson model. The single-impurity Anderson model (SIAM) features a magnetic impurity in a metallic bath and shows a crossover between local moment and Kondo regime. For numerical calculations, the continuous bath is discretized, leading to the following Hamiltonian:

$$\hat{H} = (\varepsilon_0 - \mu)(\hat{n}_\uparrow + \hat{n}_\downarrow) + U\hat{n}_\uparrow\hat{n}_\downarrow + \sum_{\ell=1}^{3} E_\ell \hat{c}_\ell^\dagger \hat{c}_\ell + \sum_{\ell=1}^{3} (V_\ell \hat{d}_\sigma^\dagger \hat{c}_\ell + \text{H.c.}). \tag{6}$$

ε_0 represents the impurity site energy, μ is the chemical potential, and U is the on-site interaction. The annihilation (creation) operator on the impurity site is $\hat{d}_\sigma^{(\dagger)}$, and $\hat{n}_\sigma = \hat{d}_\sigma^\dagger \hat{d}_\sigma$. The bath density of states is assumed to be semicircular, and the parameters V_ℓ and E_ℓ denote the hybridization strength and energy levels of the discretized bath (three levels), respectively. Figure 4(a) illustrates D_{max} of the QTT representation of $G^{\uparrow\uparrow\uparrow\uparrow}_{\text{imp}}(\tau_1, \tau_2, \tau_3)$ at the impurity site for $\beta = 100$, plotted against the model parameters U and V, where V denotes the hybridization strength in the original continuous model. In Fig. 4(b), the spin susceptibility χ_S is depicted. The red dots mark the Kondo temperature $T_K = V\sqrt{U}e^{-\pi U/8V^2}$ estimated via poor man's scaling [60,100], which delineates the boundary between Kondo and local moment regimes, as also reflected in the spin susceptibility behavior. D_{max} has a broad peak located in the vicinity of the Kondo temperature, diagnosing the thermally driven Kondo to local moments regime crossover.

Conclusions. Since their recent invention, QTTs have primarily been applied as a compression tool in numerical

calculations to overcome severe memory bottlenecks. In this work, we present a QTTD approach, diagnosing imaginary-timescale entanglement from the QTT bond dimension. By studying various models we show that timescale entanglement becomes maximal at phase transitions and crossovers, making their identification possible via QTTD. This is even true for the one-particle Green's function whose static, time-independent part does not signal a second-order phase transition when approaching it from the symmetry-unbroken side. In Green's function dynamics, the phase transition is, however, encoded in its timescale entanglement. Specifically, we identify distinct signatures of scale invariance and complexity imprinting themselves on generic correlation functions at critical points becoming accessible through QTTD. This implies that timescale entanglement is a system-inherent property. We hope that this will lead to a better understanding of how criticality and scale invariance manifest in different observables of the system.

Apart from a fresh perspective on phase transitions, and possibly other physical phenomena, the strong point of QTTD is that it can be used universally for zero and finite temperature and multiple correlation functions—it is not limited to ground-state methods and does not require specific measures or susceptibilities. Lastly, let us mention that exploring a connection to alternative notions of entanglement [101–108] and the recently introduced information lattice [109–112] that has been applied to the study of metal-insulator transitions [113] offers an exciting perspective for future work.

Acknowledgments. We thank S. Badr, G. Bellomia, J. von Delft, H. Eßl, M. Frankenbach, E. Jacob, M. Reitner, M. Ritter, and N. Ritz for insightful discussions. This work was funded in part by the Austrian Science Fund (FWF) projects through Grants DOI No. 10.55776/P36332, No. 10.55776/F86, No. 10.55776/I5868, No. 10.55776/V1018, and No. 10.55776/PIN4372024. Calculations have been partly performed using Austrian Scientific Computing (ASC). H.S. was supported by JSPS KAKENHI Grants No. 21H01041, No. 21H01003, and No. 23H03817, JSPS Bilateral Program No. JPJSBP120252002, as well as JST FOREST Grant No. JPMJFR2232, Japan. We acknowledge the use of large language models (LLMs) for assistance in the preparation of this manuscript, particularly for text editing and language refinement.

Data availability. The data that support the findings of this article are openly available [114].

[1] L. D. Landau, On the theory of phase transitions, Zh. Eksp. Teor. Fiz. **7**, 19 (1937).
[2] D. Geffroy, A. Hariki, and J. Kuneš, Excitonic magnet in external field: Complex order parameter and spin currents, Phys. Rev. B **97**, 155114 (2018).
[3] A. Niyazi, D. Geffroy, and J. Kuneš, Dynamical response and competing orders in two-band Hubbard model, Phys. Rev. B **102**, 085159 (2020).
[4] L. Amico, R. Fazio, A. Osterloh, and V. Vedral, Entanglement in many-body systems, Rev. Mod. Phys. **80**, 517 (2008).
[5] P. Laurell, A. Scheie, E. Dagotto, and D. A. Tennant, Witnessing entanglement and quantum correlations in condensed matter: A review, Adv. Quantum Technol. **8**, 2400196 (2025).
[6] R. Horodecki, P. Horodecki, M. Horodecki, and K. Horodecki, Quantum entanglement, Rev. Mod. Phys. **81**, 865 (2009).
[7] D. Bałut, X. Guo, N. d. Vries, D. Chaudhuri, B. Bradlyn, P. Abbamonte, and P. W. Phillips, Quantum Fisher information reveals UV-IR mixing in the strange metal, Physica C **635**, 1354750 (2025).
[8] F. Mazza, S. Biswas, X. Yan, A. Prokofiev, P. Steffens, Q. Si, F. F. Assaad, and S. Paschen, Quantum Fisher information in a strange metal, Nat. Phys. **22**, 1064 (2026).
[9] G. Bellomia, C. Mejuto-Zaera, M. Capone, and A. Amaricci, Quasilocal entanglement across the Mott-Hubbard transition, Phys. Rev. B **109**, 115104 (2024).
[10] C. Walsh, P. Sémon, D. Poulin, G. Sordi, and A.-M. S. Tremblay, Entanglement and classical correlations at the doping-driven Mott transition in the two-dimensional Hubbard model, PRX Quantum **1**, 020310 (2020).
[11] I. Affleck, T. Kennedy, E. H. Lieb, and H. Tasaki, Rigorous results on valence-bond ground states in antiferromagnets, Phys. Rev. Lett. **59**, 799 (1987).
[12] U. Schollwöck, The density-matrix renormalization group in the age of matrix product states, Ann. Phys. **326**, 96 (2011).
[13] J. I. Cirac, D. Pérez-García, N. Schuch, and F. Verstraete, Matrix product states and projected entangled pair states: Concepts, symmetries, theorems, Rev. Mod. Phys. **93**, 045003 (2021).
[14] J. Eisert, M. Cramer, and M. B. Plenio, *Colloquium*: Area laws for the entanglement entropy, Rev. Mod. Phys. **82**, 277 (2010).
[15] M. B. Hastings, An area law for one-dimensional quantum systems, J. Stat. Mech.: Theory Exp. (2007) P08024.
[16] Z. He and A. J. Millis, Entanglement entropy and computational complexity of the Anderson impurity model out of equilibrium: Quench dynamics, Phys. Rev. B **96**, 085107 (2017).
[17] F. A. Wolf, I. P. McCulloch, and U. Schollwöck, Solving nonequilibrium dynamical mean-field theory using matrix product states, Phys. Rev. B **90**, 235131 (2014).
[18] F. Verstraete and J. I. Cirac, Matrix product states represent ground states faithfully, Phys. Rev. B **73**, 094423 (2006).
[19] J.-W. Li and X. Waintal, Matrix product states and first quantization, Phys. Rev. Lett. **136**, 116503 (2026).
[20] I. V. Oseledets, Approximation of matrices with logarithmic number of parameters, Dokl. Math. **80**, 653 (2009).
[21] I. V. Oseledets, Tensor-train decomposition, SIAM J. Sci. Comput. **33**, 2295 (2011).
[22] B. N. Khoromskij, $O(d \log N)$-quantics approximation of $N - d$ tensors in high-dimensional numerical modeling, Constructive Approximation **34**, 257 (2011).
[23] S. Dolgov, B. Khoromskij, and D. Savostyanov, Superfast Fourier transform using QTT approximation, J. Fourier Anal. Appl. **18**, 915 (2012).

[24] B. N. Khoromskij, *Tensor Numerical Methods in Scientific computing*, 1st ed., Radon Series on Computational and Applied Mathematics Vol. 19 (De Gruyter, Berlin, 2018).

[25] N. Gourianov, M. Lubasch, S. Dolgov, Q. Y. van den Berg, H. Babaee, P. Givi, M. Kiffner, and D. Jaksch, A quantum-inspired approach to exploit turbulence structures, Nat. Comput. Sci. **2**, 30 (2022).

[26] R. D. Peddinti, S. Pisoni, A. Marini, P. Lott, H. Argentieri, E. Tiunov, and L. Aolita, Quantum-inspired framework for computational fluid dynamics, Commun. Phys. **7**, 135 (2024).

[27] E. Kornev, S. Dolgov, K. Pinto, M. Pflitsch, M. Perelshtein, and A. Melnikov, Numerical solution of the incompressible Navier-Stokes equations for chemical mixers via quantum-inspired tensor train finite element method, arXiv:2305.10784.

[28] L. Hölscher, P. Rao, L. Müller, J. Klepsch, A. Luckow, T. Stollenwerk, and F. K. Wilhelm, Quantum-inspired fluid simulation of two-dimensional turbulence with GPU acceleration, Phys. Rev. Res. **7**, 013112 (2025).

[29] N. Gourianov, P. Givi, D. Jaksch, and S. B. Pope, Tensor networks enable the calculation of turbulence probability distributions, Sci. Adv. **11**, eads5990 (2025).

[30] E. Ye and N. F. G. Loureiro, Quantum-inspired method for solving the Vlasov-Poisson equations, Phys. Rev. E **106**, 035208 (2022).

[31] N. Jolly, Y. N. Fernández, and X. Waintal, Tensorized orbitals for computational chemistry, Phys. Rev. B **111**, 245115 (2025).

[32] M. K. Ritter, Y. Núñez Fernández, M. Wallerberger, J. von Delft, H. Shinaoka, and X. Waintal, Quantics tensor cross interpolation for high-resolution parsimonious representations of multivariate functions, Phys. Rev. Lett. **132**, 056501 (2024).

[33] H. Shinaoka, M. Wallerberger, Y. Murakami, K. Nogaki, R. Sakurai, P. Werner, and A. Kauch, Multiscale space-time ansatz for correlation functions of quantum systems based on quantics tensor trains, Phys. Rev. X **13**, 021015 (2023).

[34] S. Rohshap, M. K. Ritter, H. Shinaoka, J. von Delft, M. Wallerberger, and A. Kauch, Two-particle calculations with quantics tensor trains: Solving the parquet equations, Phys. Rev. Res. **7**, 023087 (2025).

[35] See Supplemental Material at http://link.aps.org/supplemental/10.1103/znzs-rccp for additional derivations and figures supporting the conclusions reached in the publication.

[36] M. Fishman, S. White, and E. M. Stoudenmire, The ITensor software library for tensor network calculations, SciPost Phys. Codebases 4 (2022).

[37] Y. Núñez Fernández, M. Jeannin, P. T. Dumitrescu, T. Kloss, J. Kaye, O. Parcollet, and X. Waintal, Learning Feynman diagrams with tensor trains, Phys. Rev. X **12**, 041018 (2022).

[38] Y. Núñez Fernández, M. K. Ritter, M. Jeannin, J.-W. Li, T. Kloss, T. Louvet, S. Terasaki, O. Parcollet, J. von Delft, H. Shinaoka, and X. Waintal, Learning tensor networks with tensor cross interpolation: New algorithms and libraries, SciPost Phys. **18**, 104 (2025).

[39] M. K. Ritter, Fast elementwise operations on tensor trains with alternating cross interpolation, arXiv:2604.00037.

[40] S. Rohshap, J.-W. Li, A. Lorenz, S. Hasil, K. Held, A. Kauch, and M. Wallerberger, Entanglement across scales: Quantics tensor trains as a natural framework for renormalization, Phys. Rev. Res. **7**, 043313 (2025).

[41] H. Ishida, N. Okada, S. Hoshino, and H. Shinaoka, Low-rank quantics tensor train representations of Feynman diagrams for multiorbital electron-phonon models, Phys. Rev. Lett. **135**, 046502 (2025).

[42] M. Murray, H. Shinaoka, and P. Werner, Nonequilibrium diagrammatic many-body simulations with quantics tensor trains, Phys. Rev. B **109**, 165135 (2024).

[43] H. Takahashi, R. Sakurai, and H. Shinaoka, Compactness of quantics tensor train representations of local imaginary-time propagators, SciPost Phys. **18**, 007 (2025).

[44] A. Erpenbeck, W.-T. Lin, T. Blommel, L. Zhang, S. Iskakov, L. Bernheimer, Y. Núñez-Fernández, G. Cohen, O. Parcollet, X. Waintal, and E. Gull, Tensor train continuous time solver for quantum impurity models, Phys. Rev. B **107**, 245135 (2023).

[45] M. Eckstein, Solving quantum impurity models in the nonequilibrium steady state with tensor trains, arXiv:2410.19707.

[46] M. Środa, K. Inayoshi, H. Shinaoka, and P. Werner, Memory-efficient nonequilibrium Green's function framework built on quantics tensor trains, Phys. Rev. Lett. **135**, 226501 (2025).

[47] M. Frankenbach, M. Ritter, M. Pelz, N. Ritz, J. von Delft, and A. Ge, Compressing local vertex functions from the multipoint numerical renormalization group using quantics tensor cross interpolation, Phys. Rev. Res. **7**, 043032 (2025).

[48] G. Grosso, M. K. Ritter, S. Rohshap, S. Badr, A. Kauch, M. Wallerberger, J. von Delft, and H. Shinaoka, Adaptive patching for tensor train computations, arXiv:2602.22372.

[49] H.-Y. Lee and N. Kawashima, Quantics tensor trains for multiloop functional renormalization group in multiorbital impurity models, arXiv:2610.29341.

[50] H. Eßl, S. Rohshap, M. Gievers, M. Wallerberger, A. Toschi, and A. Kauch, Stabilizing the parquet problem, arXiv:2606.04936.

[51] M. Gievers, H. Eßl, S. Rohshap, A. Kauch, and A. Toschi, Instabilities in self-consistent diagrammatic approaches and how to cure them, arXiv:2609.11405.

[52] M. Wallerberger and K. Held, Trie-based ranking of quantum many-body states, Phys. Rev. Res. **4**, 033238 (2022).

[53] S. Nishimoto, K. Sano, and Y. Ohta, Phase diagram of the one-dimensional Hubbard model with next-nearest-neighbor hopping, Phys. Rev. B **77**, 085119 (2008).

[54] L. Wang, Y.-H. Liu, J. Imriška, P. N. Ma, and M. Troyer, Fidelity susceptibility made simple: A unified quantum Monte Carlo approach, Phys. Rev. X **5**, 031007 (2015).

[55] P. Zanardi and N. Paunković, Ground state overlap and quantum phase transitions, Phys. Rev. E **74**, 031123 (2006).

[56] W.-L. You, Y.-W. Li, and S.-J. Gu, Fidelity, dynamic structure factor, and susceptibility in critical phenomena, Phys. Rev. E **76**, 022101 (2007).

[57] P. Zanardi, P. Giorda, and M. Cozzini, Information-theoretic differential geometry of quantum phase transitions, Phys. Rev. Lett. **99**, 100603 (2007).

[58] L. Campos Venuti and P. Zanardi, Quantum critical scaling of the geometric tensors, Phys. Rev. Lett. **99**, 095701 (2007).

[59] T. Kashihara, Y. Michishita, and R. Peters, Quantum metric on the Brillouin zone in correlated electron systems and its relation to topology for Chern insulators, Phys. Rev. B **107**, 125116 (2023).

[60] L. Wang, H. Shinaoka, and M. Troyer, Fidelity susceptibility perspective on the Kondo effect and impurity quantum phase transitions, Phys. Rev. Lett. **115**, 236601 (2015).

[61] P. Hauke, M. Heyl, L. Tagliacozzo, and P. Zoller, Measuring multipartite entanglement through dynamic susceptibilities, Nat. Phys. **12**, 778 (2016).

[62] S. Qu, F.-Q. Xu, B. Guo, and Z.-Y. Sun, Quantum Fisher information in one-dimensional translation-invariant quantum systems: Large-N limit analysis, Phys. Lett. A **529**, 130103 (2025).

[63] W. H. Zurek, Information transfer in quantum measurements: Irreversibility and amplification, in *Quantum Optics, Experimental Gravity, and Measurement Theory*, edited by P. Meystre and M. O. Scully (Springer, Boston, 1983), pp. 87–116.

[64] S. M. Barnett and S. J. D. Phoenix, Entropy as a measure of quantum optical correlation, Phys. Rev. A **40**, 2404 (1989).

[65] G. Roósz, A. Kauch, F. Bippus, D. Wieser, and K. Held, Two-site reduced density matrix from one- and two-particle Green's functions, Phys. Rev. B **110**, 075115 (2024).

[66] F. Bippus, J. Krsnik, M. Kitatani, L. Akšamović, A. Kauch, N. Barišić, and K. Held, Entanglement in the pseudogap regime of cuprate superconductors, Phys. Rev. B **112**, L081110 (2025).

[67] F. Bippus, A. Kauch, G. Roósz, C. Mayrhofer, F. Assaad, and K. Held, Two-site entanglement in the two-dimensional Hubbard model, Phys. Rev. B **113**, 035152 (2026).

[68] T. Grover, Entanglement of interacting fermions in quantum Monte Carlo calculations, Phys. Rev. Lett. **111**, 130402 (2013),.

[69] A. Rényi, On measures of entropy and information, in *Proceedings of the Fourth Berkeley Symposium on Mathematical Statistics and Probability, Volume 1: Contributions to the Theory of Statistics* (University of California Press, Oakland, 1961), Vol. 4.1, pp. 547–562.

[70] A. Peres, Separability criterion for density matrices, Phys. Rev. Lett. **77**, 1413 (1996).

[71] M. Horodecki, P. Horodecki, and R. Horodecki, Separability of mixed states: Necessary and sufficient conditions, Phys. Lett. A **223**, 1 (1996).

[72] G. De Chiara and A. Sanpera, Genuine quantum correlations in quantum many-body systems: A review of recent progress, Rep. Prog. Phys. **81**, 074002 (2018).

[73] Y.-D. Zheng and B. Zhou, Negativity and quantum phase transition in a mixed spin-(12, 52, 12) Ising–Heisenberg branched chain, Physica A **603**, 127753 (2022).

[74] P. Das and A. Sharma, Revisiting the phase transitions of the Dicke model, Phys. Rev. A **105**, 033716 (2022).

[75] S. Yamashika, S. Endo, and H. Tajima, Quantum Fisher information as a measure of symmetry breaking in quantum many-body systems, arXiv:2509.07468.

[76] G. Bellomia, A. Amaricci, and M. Capone, Local classical correlations between physical electrons in Hubbard systems, Phys. Rev. B **113**, 155158 (2026).

[77] G. B. Mbeng, A. Russomanno, and G. E. Santoro, The quantum Ising chain for beginners, SciPost Phys. Lect. Notes 82 (2024).

[78] G. Vidal, J. I. Latorre, E. Rico, and A. Kitaev, Entanglement in quantum critical phenomena, Phys. Rev. Lett. **90**, 227902 (2003).

[79] G. Vidal, Entanglement renormalization, Phys. Rev. Lett. **99**, 220405 (2007).

[80] G. Vidal, Class of quantum many-body states that can be efficiently simulated, Phys. Rev. Lett. **101**, 110501 (2008).

[81] G. M. Crosswhite, A. C. Doherty, and G. Vidal, Applying matrix product operators to model systems with long-range interactions, Phys. Rev. B **78**, 035116 (2008).

[82] R. N. C. Pfeifer, G. Evenbly, and G. Vidal, Entanglement renormalization, scale invariance, and quantum criticality, Phys. Rev. A **79**, 040301 (2009).

[83] B. Pirvu, G. Vidal, F. Verstraete, and L. Tagliacozzo, Matrix product states for critical spin chains: Finite-size versus finite-entanglement scaling, Phys. Rev. B **86**, 075117 (2012).

[84] J. Haegeman, T. J. Osborne, H. Verschelde, and F. Verstraete, Entanglement renormalization for quantum fields in real space, Phys. Rev. Lett. **110**, 100402 (2013).

[85] B. Vanhecke, J. Haegeman, K. Van Acoleyen, L. Vanderstraeten, and F. Verstraete, Scaling hypothesis for matrix product states, Phys. Rev. Lett. **123**, 250604 (2019).

[86] K. Van Acoleyen, A. Hallam, M. Bal, M. Hauru, J. Haegeman, and F. Verstraete, Entanglement compression in scale space: From the multiscale entanglement renormalization ansatz to matrix product operators, Phys. Rev. B **102**, 165131 (2020).

[87] W. Metzner and D. Vollhardt, Correlated lattice fermions in $d = \infty$ dimensions, Phys. Rev. Lett. **62**, 324 (1989).

[88] A. Georges and G. Kotliar, Hubbard model in infinite dimensions, Phys. Rev. B **45**, 6479 (1992).

[89] A. Georges, G. Kotliar, W. Krauth, and M. J. Rozenberg, Dynamical mean-field theory of strongly correlated fermion systems and the limit of infinite dimensions, Rev. Mod. Phys. **68**, 13 (1996).

[90] M. Wallerberger, A. Hausoel, P. Gunacker, A. Kowalski, N. Parragh, F. Goth, K. Held, and G. Sangiovanni, w2dynamics: Local one- and two-particle quantities from dynamical mean field theory, Comput. Phys. Commun. **235**, 388 (2019).

[91] C. Watzenböck, M. Fellinger, K. Held, and A. Toschi, Long-term memory magnetic correlations in the Hubbard model: A dynamical mean-field theory analysis, SciPost Phys. **12**, 184 (2022).

[92] C. U. Watzenböck, Vertex corrections in strongly correlated electron systems - timescales of the spin and charge response, Ph.D. thesis, 2022.

[93] Enhancement of timescale entanglement can also be observed in the plain one-particle Green's function $G(i\nu)$ but becomes more explicit in the particle-hole bubble through enhanced scale mixing.

[94] L. M. Verhoff, L. Si, and K. Held, Surfaces and interfaces of infinite-layer nickelates studied by dynamical mean-field theory, Phys. Rev. B **112**, 195122 (2025).

[95] P. Blaha, K. Schwarz, F. Tran, R. Laskowski, G. K. H. Madsen, and L. D. Marks, WIEN2k: An APW+lo program for calculating the properties of solids, J. Chem. Phys. **152**, 074101 (2020).

[96] G. Pizzi, V. Vitale, R. Arita, S. Blügel, F. Freimuth, G. Géranton, M. Gibertini, D. Gresch, C. Johnson, T. Koretsune, J. Ibañez-Azpiroz, H. Lee, J.-M. Lihm, D. Marchand, A. Marrazzo, Y. Mokrousov, J. I. Mustafa, Y. Nohara, Y. Nomura, L. Paulatto, *et al.*, Wannier90 as a community code: New features and applications, J. Phys.: Condens. Matter **32**, 165902 (2020).

[97] J. Kuneš, R. Arita, P. Wissgott, A. Toschi, H. Ikeda, and K. Held, Wien2wannier: From linearized augmented plane waves to maximally localized Wannier functions, Comput. Phys. Commun. **181**, 1888 (2010).

[98] J. Kaufmann and K. Held, ana_cont: Python package for analytic continuation, Comput. Phys. Commun. **282**, 108519 (2023).

[99] Zigzag of bond dimensions caused by different inter- and intrascale entanglement between variables in interleaved QTT representation.

[100] F. Haldane, Scaling theory of the asymmetric Anderson model, Phys. Rev. Lett. **40**, 416 (1978).

[101] V. Balasubramanian, M. B. McDermott, and M. Van Raamsdonk, Momentum-space entanglement and renormalization in quantum field theory, Phys. Rev. D **86**, 045014 (2012).

[102] M. H. Martins Costa, J. van den Brink, F. S. Nogueira, and G. I. Krein, Momentum space entanglement from the Wilsonian effective action, Phys. Rev. D **106**, 065024 (2022).

[103] K. Doi, J. Harper, A. Mollabashi, T. Takayanagi, and Y. Taki, Timelike entanglement entropy, J. High Energy Phys. 04 (2023) 052.

[104] K. Doi, J. Harper, A. Mollabashi, T. Takayanagi, and Y. Taki, Pseudoentropy in dS/CFT and timelike entanglement entropy, Phys. Rev. Lett. **130**, 031601 (2023).

[105] S. Grieninger, K. Ikeda, and D. E. Kharzeev, Temporal entanglement entropy as a probe of renormalization group flow, J. High Energy Phys. 05 (2024) 030.

[106] O. A. Castro-Alvaredo, Temporal entanglement in quantum field theory, J. Phys. A **59**, 355201 (2026).

[107] J. Maldacena, The large-*N* limit of superconformal field theories and supergravity, Int. J. Theor. Phys. **38**, 1113 (1999).

[108] B. Swingle, Entanglement renormalization and holography, Phys. Rev. D **86**, 065007 (2012).

[109] T. Klein Kvorning, L. Herviou, and J. H. Bardarson, Time-evolution of local information: Thermalization dynamics of local observables, SciPost Phys. **13**, 080 (2022).

[110] C. Artiaco, C. Fleckenstein, D. Aceituno Chávez, T. K. Kvorning, and J. H. Bardarson, Efficient large-scale many-body quantum dynamics via local-information time evolution, PRX Quantum **5**, 020352 (2024).

[111] C. Artiaco, T. Klein Kvorning, D. Aceituno Chávez, L. Herviou, and J. H. Bardarson, Universal characterization of quantum many-body states through local information, Phys. Rev. Lett. **134**, 190401 (2025).

[112] N. P. Bauer, B. Trauzettel, T. Klein Kvorning, J. H. Bardarson, and C. Artiaco, Local information flow in quantum quench dynamics, Phys. Rev. A **112**, 022221 (2025).

[113] W. Skoglund, E. Giacomelli, Y. Yang, J. H. Bardarson, and E. van Loon, Information lattice approach to the metal-insulator transition, Phys. Rev. Res. **8**, 023102 (2026).

[114] S. Rohshap, H. Ishida, F. Bippus, L. M. Verhoff, A. K. Kauch, K. Held, H. Shinaoka, and M. Wallerberger, Data for "Diagnosing phase transitions through time-scale entanglement" [Dataset], TU Wien, 2026, https://doi.org/10.48436/3z1va-52745.